



HAL
open science

Fatigue characterization by heat source reconstruction under continuously varying stress amplitude

Corentin Douellou, Xavier Balandraud, Emmanuel Duc

► **To cite this version:**

Corentin Douellou, Xavier Balandraud, Emmanuel Duc. Fatigue characterization by heat source reconstruction under continuously varying stress amplitude. *International Journal of Fatigue*, 2022, 159, pp.106782. 10.1016/j.ijfatigue.2022.106782 . hal-04004959

HAL Id: hal-04004959

<https://hal.science/hal-04004959>

Submitted on 25 Feb 2023

HAL is a multi-disciplinary open access archive for the deposit and dissemination of scientific research documents, whether they are published or not. The documents may come from teaching and research institutions in France or abroad, or from public or private research centers.

L'archive ouverte pluridisciplinaire **HAL**, est destinée au dépôt et à la diffusion de documents scientifiques de niveau recherche, publiés ou non, émanant des établissements d'enseignement et de recherche français ou étrangers, des laboratoires publics ou privés.

Fatigue characterization by heat source reconstruction under continuously varying stress amplitude

Corentin Douellou^a, Xavier Balandraud^{a,*}, Emmanuel Duc^a

^a Université Clermont Auvergne, Clermont Auvergne INP, CNRS, Institut Pascal, F-63000 Clermont-Ferrand, France

* Corresponding author.

E-mail addresses:

corentin.douellou@sigma-clermont.fr (A. Douellou),

xavier.balandraud@sigma-clermont.fr (X. Balandraud),

emmanuel.duc@sigma-clermont.fr (E. duc).

Abstract

Self-heating measurements using thermography have proven to be an effective means of rapidly assessing the fatigue response of materials. The paper validates the use of a post-processing technique, called "heat source" reconstruction, in the case of cyclic loading with *continuously varying* stress amplitudes, offering significant advantages over classical self-heating approaches: considerably reduced test time (some minutes compared to a few hours); continuous measurement of mechanical dissipation versus stress amplitude; higher maximum stress amplitude achieved due to slower accumulation of fatigue damage during testing. The approach was validated by comparison with the classical procedure, and opens new perspectives for fatigue characterization.

Keywords: infrared thermography; dissipation; self-heating; additive manufacturing; steel

1. Introduction

Conventional fatigue characterization, such as Wöhler curves or staircases, involves long and costly testing. Typically, 20 to 30 specimens and several weeks of testing are required to build a Wöhler curve. However, procedures for the rapid determination of a material's fatigue limit have also been developed, such as the physically-based lifetime calculation (PhyBaL) method [1, 2] or methods based on self-heating. In the early twentieth century, Stromeier showed that cyclic mechanical loading is accompanied by material self-heating [3]. Basing themselves on this effect, Luong, as well as La Rosa and Risitano, proposed in the late 1990s a fast procedure for fatigue limit evaluation using infrared (IR) thermography [4-7]. The general idea is to apply a series of cyclic loading blocks at *constant* stress amplitudes, increasing until specimen failure, and to distinguish two regimes in the measured thermal response, namely below and above the material's fatigue limit. Generally, the duration of each loading block at constant amplitude is of some minutes in order to reach a stabilized temperature (temperature plateau), if such a plateau exists. Furthermore, a waiting time can be applied between the loading blocks in order to return to ambient temperature. It is thus possible to identify the fatigue limit of a material from a single specimen in a few hours, the duration depending on the number of stress amplitudes considered. Identifying the separation between the two thermal regimes is, however, complex. Different criteria have been compared in the literature; see for instance Ref [8]. The temperature plateau as a robust parameter to investigate the fatigue limit of steels was also discussed in Ref [9]. Studies have been also carried out on the understanding of the physical mechanisms related to self-heating, namely the progressive appearance of micro-plasticity during cyclic loading [10, 11]. Approaches based on self-heating measurements, including heat dissipation calculation, have been successfully applied to various materials such as steels [9-23], aluminum alloys [23, 24], magnesium alloys [25-27], copper and copper alloys [28-30], titanium alloys [31], nickel-titanium shape memory alloys [32-35], ceramics [36] and composite materials [37-40].

It is well known that temperature changes during a mechanical test are not related only to deformation mechanisms in the material. Indeed, heat diffusion within the specimen and heat exchanges with the environment (ambient air, jaws of the testing machine) alter the temperature fields. In the late 1980s, Chrysochoos developed heat source reconstruction (HSR) techniques, based on the heat diffusion equation, to retrieve the calorific origin of the temperature changes

in the specimen under mechanical loading [41, 42]. The term “heat source” designates here the heat power density (in W/m^3) produced or absorbed by the material due to a change in its mechanical state. The approach can be described as “deformation calorimetry”. While the heat diffusion equation is classically used in finite element simulations to calculate temperature fields from the knowledge of thermal boundary conditions and heat sources, HSR aims to do the opposite: calculating heat sources within the specimen from the knowledge of the measured temperature variations. In practice, temperatures are acquired at the surface of the specimen by IR thermography, which requires specific versions of the heat diffusion equation, applicable for instance to thin or elongated specimens [43, 44]. It is worth noting that the heat sources are composed of a thermo-elastic coupling contribution and *mechanical dissipation* (also named *intrinsic dissipation*). The latter calorific quantity is associated with any irreversible mechanical phenomena such as plasticity, friction, viscosity, cracking or fatigue damage, depending on the loading conditions and the type of material. For fatigue characterization, HSR can be used to identify the calorific origin of self-heating, *i.e.* the mechanical dissipation. In this context, HSR has been applied to the study of the fatigue for various types of materials, such as steels [45-48], aluminum alloys [49, 50], copper and brass [51, 52] and reinforced plastics [53-55]. In general, the advantage of using HSR is that it enables the analysis of a quantity which is intrinsically linked to fatigue damage (mechanical dissipation) as opposed to temperature variations, which depend in part on heat exchanges with the specimen's environment.

In our previous study in Ref [56], HSR was applied to the fatigue characterization of an additive manufacturing (AM) steel. We evaluated the increase in mechanical dissipation as a function of stress amplitude using the classical loading procedure, *i.e.* a series of cyclic blocks at *constant* stress amplitudes. We compared the identified fatigue limit obtained with that obtained from conventional fatigue tests (Wöhler curve). This work showed that HSR enables a reliable and precise identification of the material's fatigue limit. However, we believe that the potential of HSR for fatigue characterization can be revealed by applying another, even faster loading procedure. The objective of the present study is to perform HSR in the case of cyclic loading at *continuously varying* stress amplitude (instead of a series of loading blocks at constant amplitudes as in the classical approach) in order to obtain a *continuous* relationship between mechanical dissipation and stress amplitude. Other advantages will be presented in the course of the paper.

In order to validate the new approach proposed, we applied it to specimens identical to those used in our earlier work [56]. These AM specimens were made using Laser Powder Bed Fusion (L-PBF) by the AddUp company, Cébazat, France. Two types of steel were tested. The first one was 18Ni300 Maraging – a portmanteau word for “martensite” and “aging” – steel. This material is quite common in the metallic L-PBF field, since it combines good weldability and interesting mechanical properties (high strength and good ductility) after aging heat treatment. Two porosity levels were compared in the present study. The second material was Nanosteel L40-BLDRMetal steel. L40 is a tool steel with high tenacity and toughness, also well known for being adapted to L-PBF manufacturing. L40 is attractive for highly demanding industries such as defense or aerospace, due to the good mechanical properties that can be achieved with this manufacturing technology. However, the fatigue behavior of additively manufactured parts is identified as being a sensitive issue. Being able to quickly (in some minutes) characterize the fatigue performance of AM materials would be of great benefit to designers and manufacturers in their search for optimized manufacturing parameters. Note finally that the main objective of the present study is not to identify the fatigue limit values of the different materials tested, but to show that the proposed new procedure enables a continuous and rapid assessment of the relationship between mechanical dissipation and stress amplitude. However, the identification of the fatigue limits of the tested materials will be discussed in the paper.

The paper is structured as follows. Section 2 presents the experimental setup, in particular the new loading procedure and the specimen geometry. Section 3 is a background on HSR and the evaluation of mechanical dissipation during fatigue tests. Section 4 presents a preliminary numerical simulation to illustrate the thermal phenomena involved during a fatigue test at *continuously varying* stress amplitude. Section 5 presents the results for the maraging and L40 steels. These results are compared with those obtained from the classical loading procedure (series of loading blocks at constant amplitudes). Finally, Section 6 is dedicated to comments about the data processing.

2. Experimental setup

2.1. New loading procedure

As explained in the introduction, the classical study of self-heating under cyclic loading enables a fast identification of the material's fatigue limit (in a few hours). The main purpose of the present paper is to propose and study a new loading procedure for an even faster fatigue characterization by post-processing the thermal data using HSR. Figure 1 shows the proposed mechanical loading in which the force amplitude linearly increases through time. In the present study, the maximum stress σ_{\max} was increased by 0.1 MPa at each cycle. The load ratio R and the load frequency f_L were fixed to 0.1 and to 30 Hz respectively, as in our previous study [56] using the classical loading procedure for comparison. It can be noted in Fig. 1 that the first cycle was set to $\sigma_{\max} = 50$ MPa rather than zero. This was done to avoid potential buckling at the start of the test.

As will be shown from the experimental results, higher stress amplitudes can be reached by the proposed new loading procedure compared to the classical one. Indeed, the accumulation of fatigue damage is much slower as it is not necessary to wait for a temperature plateau at each stress amplitude. We chose to stop the tests when σ_{\max} reached 90% of the 0.2% offset yield strength ($Rp_{0.2}$) of the material for safety considerations.

By construction, no temperature stabilization is expected under this cyclic loading at continuously varying amplitude: the classical method cannot be applied. HSR is proposed in the present study to obtain a *continuous* relationship between mechanical dissipation and stress amplitude.

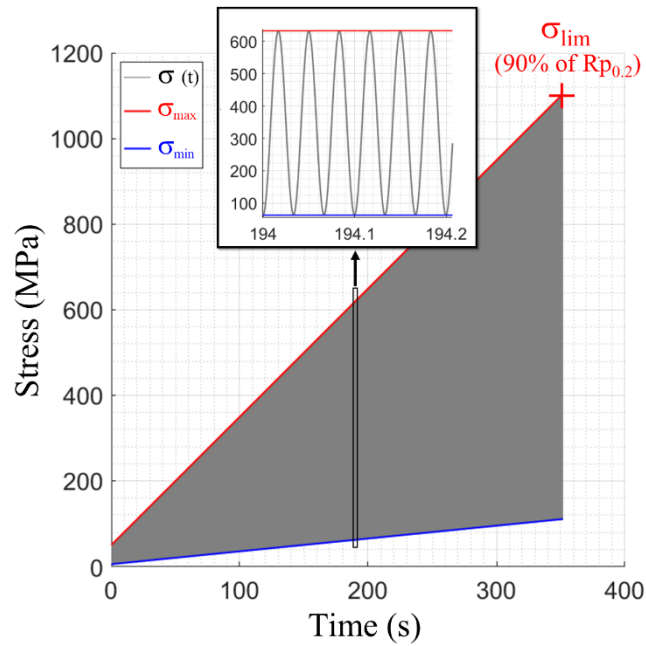


Fig. 1 Mechanical loading.

2.2. Loading setup and thermal measurement

Figure 2-a shows the experimental setup. Cyclic tensile loading was applied using a ± 15 kN MTS testing machine. Thermal measurements were made with a Cedip Jade III MWIR camera featuring a Noise Equivalent Temperature Difference (NETD) of 0.02°C at ambient temperature. The acquisition frequency f_A and integration time were set to 100 Hz and 1500 μs respectively. Note that particular attention was paid to protecting the specimen from external heat disturbances. A tunnel and thick black curtains surrounded the environment from the IR camera to the specimen, to limit both radiative and convective perturbations. Thermocouples were used to monitor temperatures in the facility during testing. Specimens were painted with a thin layer of matte black paint to maximize thermal emissivity. The specimen geometry was in agreement with the ISO 1099:2017 standard: flat specimens 1 mm thick with gauge zones 10 mm wide and 40 mm long connected by fillets to the heads. Note that a “thin” specimen (a few millimeters at most) is required here in the framework of the HSR technique to consider that the temperature is nearly homogeneous in the thickness. As shown in Fig. 2-b, the specimens also featured two additional “reference” zones, as proposed in Ref [57]. These references enabled us to track the slight temperature variations in the specimen’s close environment during the test. It was then possible to precisely measure the changes in temperature due to the changes in the mechanical state of the specimen’s gauge zone (see details

in Section 3.4). Figure 2-c shows an example of a temperature map and the corresponding temperature changes with respect to the initial state before mechanical loading. Temperatures are higher in the upper part of the specimen due to the presence of the hydraulic actuator. It can be seen that the temperature change map is not homogeneous, due to the test machine jaws, which are heat sinks. HSR aims to retrieve the calorific origin of the temperature changes due only to the changes in the mechanical state of the material. In this context, it is necessary to track temperature variations in the grips of the test machine. Water-cooling of the mobile grip could also facilitate the processing of the thermal data, as was performed in Ref [23]. Particular attention must be paid to the heat exchange between the specimen and its environment. These conditions must be as stable as possible. To ensure this, the test machine was turned on several hours in advance of testing. A waiting time of about 10 minutes was also observed after placing the specimen in the jaws in order to reach a stable thermal state before starting mechanical loading. Finally, note that the IR camera was turned on over three hours prior to measurements to ensure a stable internal temperature.

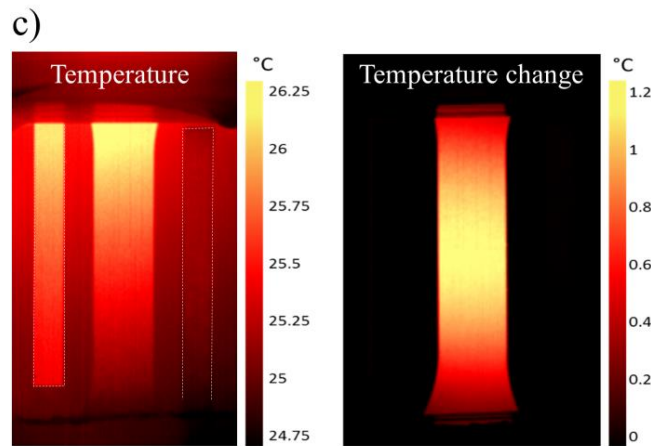
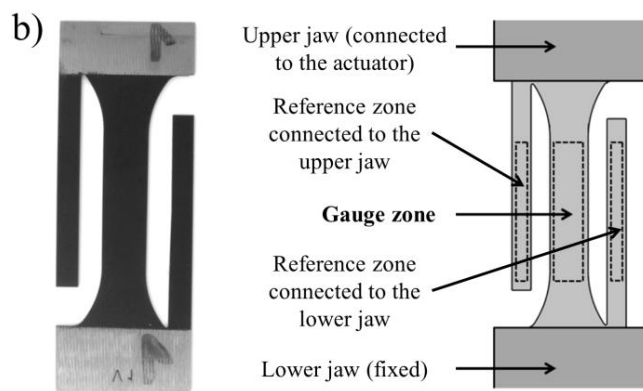


Fig. 2 a) Experimental setup, b) specimen, c) example of thermal maps under fatigue

2.3. Materials and specimens

Table 1 lists the additively-manufactured specimens tested using the loading procedure presented in Fig. 1:

- three 18Ni300 maraging specimens with low porosity (type A) – Results were compared with thirteen data sets obtained with the classical loading procedure in our previous work (Ref [56]);
- one 18Ni300 maraging specimen with a higher porosity level (type B) – Results were compared with three data sets obtained with the classical procedure in Ref [56];
- two L40 specimens – Results were compared with three data sets obtained with the classical procedure.

The difference in porosity levels between type-A and type-B specimens is due to the manufacturing strategy. The first strategy aims to optimize mechanical properties, while the second aims to maximize manufacturing productivity for part areas not subject to high mechanical stress. Table 1 gives the 0.2% offset yield strength ($Rp_{0.2}$) of the materials [58]. Finally, Table 2 provides the density ρ , specific heat C and coefficient of thermal expansion α of the two materials [58], that will be used for HSR processing.

Table 1 List and details of the AM specimens tested.

Material	Type	Manufacturing strategy	Yield strength	Number of specimens	
			$Rp_{0.2}$	with the proposed new procedure	with the classical procedure
Maraging	A	For minimum defect density (low porosity)	1260 MPa	3	13 [Douellou et al. 2020]
	B	For rapid manufacturing (higher porosity)	600 MPa	1	3 [Douellou et al. 2020]
L40		For minimum defect density (low porosity)	1331 MPa	2	6

Table 2 Thermophysical properties of the two types of steel tested.

	ρ (kg/m ³)	C (J/kg.K)	α (K ⁻¹)	τ (s)
Maraging	8100	440	11.8 10 ⁻⁶	45
L40	7780	442	11.2 10 ⁻⁶	48

3. Mechanical dissipation calculation

This section presents the thermal data processing used to calculate mechanical dissipation associated with fatigue damage. Section 3.1 is the background about thermomechanics and the principle of HSR. Sections 3.2 and 3.3 are dedicated to mechanical dissipation evaluation in the case of cyclic loading at constant amplitude and continuously varying amplitude, respectively. Section 3.4 provides information on measurement resolution.

3.1. Thermomechanics and HSR background

Any change in the mechanical state of a material is associated with a release or absorption of heat. The corresponding heat power density s (in W/m^3), named “heat source”, is actually composed of two parts [43, 44]:

- one part is associated with thermomechanical couplings, which are limited to a *thermo-elastic coupling* in most materials. For isotropic materials, the thermo-elastic coupling heat source s_{TE} can be expressed by Eq. (1), where σ_h is the hydrostatic stress and T the temperature [59]. In the case of a uniaxial loading, σ_h is equal to one third of the uniaxial stress σ , so $\sigma_h = \sigma/3$. As T is expressed in Kelvin, it can be considered as constant for variations of a few degrees. The minus sign in Eq. (1) shows that loading and unloading lead to heat absorption (temperature decrease) and heat release (temperature increase) respectively. It can finally be noted that the corresponding heat over a thermodynamic cycle is null. More specifically, s_{TE} is null on average over a loading cycle during a fatigue test at *constant* stress amplitude.

$$s_{\text{TE}} = -3 \alpha T \frac{d\sigma_h}{dt} \quad (1)$$

- the other part is the *mechanical dissipation*, or *intrinsic dissipation*, which is often denoted d_1 to be distinguished from the thermal diffusion d_2 (both terms appearing in the Clausius-Duhem inequality $d_1 + d_2 \geq 0$). It is associated with irreversible mechanisms such as plasticity, viscosity, or fatigue damage as in the present study. Mechanical dissipation (in W/m^3) is the calorific origin of the self-heating (in $^\circ\text{C}$) during a fatigue test. It is always positive: $d_1 \geq 0$.

Thus,

$$s = s_{TE} + d_1 \quad (2)$$

HSR is based on the heat diffusion equation. Several formulations of this equation can be used from experimental thermal data obtained by IR thermography at the surface of the material specimen. The reader can refer to Ref [44] for these different formulations. In the present work, the so-called zero-dimensional (0D) version can be applied. The 0D approach consists in using the temperature change *averaged* over the gauge zone of the specimen, denoted θ in the following. Its validity was discussed in Ref [28]. It can be recalled that the 0D approach does not require the temperatures within the specimen to be homogenous; it requires the spatial homogeneity of the heat sources. It was applied for instance in Refs [45, 50, 53]. In the present case, as there is no stress concentration in the gauge zone of the specimen, s_{TE} can be considered as homogeneous. The same was considered for the mechanical dissipation d_1 . Homogeneity is assumed at the scale of the specimen, even though stress localizations probably exist around porosities. Equation (3) gives the 0D version of the heat equation:

$$s = \rho C \left(\frac{d\theta}{dt} + \frac{\theta}{\tau} \right) \quad (3)$$

where τ is a time constant characterizing the heat exchanges between the specimen and its environment (ambient air and jaws of the testing machine). Its value depends on the material's thermal conductivity, but also on its geometry through the surface-to-volume ratios of the zones in contact with ambient air and with the jaws. The value of τ shall be preliminary identified by considering for instance a natural return to ambient temperature, the specimen being clamped in the jaws but without axial mechanical loading. Indeed, the solution to Eq. (3) for $s = 0$ is an exponential function whose decay constant is τ . The latter can therefore easily be identified from the experimental temperature decrease measured during a natural return to ambient temperature. Table 2 gives the values identified for the two types of material specimens.

3.2. Mechanical dissipation calculation at constant stress amplitude

Basically, HSR enables us to calculate the heat source s , which is the sum of s_{TE} and d_1 , during a mechanical test from the knowledge of θ using Eq. (3). In the context of fatigue characterization, the question is then: how to isolate the mechanical dissipation d_1 ? The answer is simple for cyclic loading at *constant* amplitude. As already mentioned, the thermo-elastic coupling heat source s_{TE} is null on average over a thermodynamic cycle, and thus over an integer number n of cycles: $\langle s_{TE} \rangle = 0$, where the angled brackets mean:

$$\langle x \rangle = \frac{1}{n} \int^{n \text{ cycles}} x dt \quad (4)$$

Thus the time average of s over an integer number n of cycles directly gives the average mechanical dissipation: $\langle d_1 \rangle = \langle s \rangle$. The average mechanical dissipation can then be directly obtained from the temperature changes measured by the IR camera as follows:

$$\langle d_1 \rangle = \langle \rho C \left(\frac{d\theta}{dt} + \frac{\theta}{\tau} \right) \rangle \quad (5)$$

Another possibility to calculate $\langle d_1 \rangle$ consists in using the average value $\langle \theta \rangle$ of the temperature change every n cycles:

$$\langle d_1 \rangle = \rho C \left(\frac{d\langle \theta \rangle}{dt} + \frac{\langle \theta \rangle}{\tau} \right) \quad (6)$$

Equations (5) and (6) are theoretically equivalent. The latter is simpler to use when the IR camera allows the real-time acquisition of the average every n cycles, which is possible with the IR camera used in this study. In practice, this solution leads to much smaller-sized thermal data files recorded from the IR camera, enabling much longer tests to be post-processed.

3.3. Case of continuously varying stress amplitude

In the case of the proposed new loading procedure (see Fig. 1), the stress amplitude is non-constant. Therefore $\langle s_{TE} \rangle \neq 0$. Nevertheless, the time average over an integer number of cycles is still useful, but the thermo-elastic contribution must be subtracted:

$$\langle d_1 \rangle = \langle s \rangle - \langle s_{TE} \rangle \quad (7)$$

where

$$\langle s \rangle = \langle \rho C \left(\frac{d\theta}{dt} + \frac{\theta}{\tau} \right) \rangle \quad (8)$$

or

$$\langle s \rangle = \rho C \left(\frac{d\langle \theta \rangle}{dt} + \frac{\langle \theta \rangle}{\tau} \right) \quad (9)$$

Equations (8) and (9) are theoretically equivalent. A comparison between these two post-processing procedures will however be discussed in Section 6. The mean thermo-elastic contribution $\langle s_{TE} \rangle$ for temperature variations of a few degrees (T being nearly constant in Kelvin) can be calculated from the following equation:

$$\langle s_{TE} \rangle = -3 \alpha T_0 \frac{d\langle \sigma_h \rangle}{dt} \quad (10)$$

where T_0 is the overall temperature in Kelvin of the specimen during the test, which can also be considered as equal to the ambient temperature. For the loading shown in Fig. 1, $d\langle \sigma_h \rangle/dt$ is constant, so $\langle s_{TE} \rangle$ is also constant. Note that $\langle s_{TE} \rangle$ can be experimentally identified at the beginning of the test (at the lowest loading levels), assuming that mechanical dissipation is negligible.

3.4. Measurement resolution

Temperature measurements are unavoidably noisy. Before presenting the results for fatigue tests, this section presents an identification of the measurement resolution of the heat source $\langle s \rangle$ in a simple case, with no mechanical loading applied to the specimen. $\langle s \rangle$ should be equal to zero. The fluctuation in the identified values of $\langle s \rangle$ thus gives information about the measurement resolution of the heat sources using HSR.

The specimen was simply clamped in the jaws of the testing machine without axial mechanical loading. The thermal acquisition frequency f_A was set to 100 Hz as in the fatigue tests. Figure 3-a shows the temperature variation over 6 minutes (after waiting more than 10 minutes after placing the specimen in the machine). Four quantities are plotted against time:

- T_{gauge} , $T_{\text{ref up}}$ and $T_{\text{ref low}}$ are the spatially-averaged temperatures over the gauge zone, the reference zone connected to the lower jaw and that connected to the upper jaw, respectively. It can be noted that the noise is much lower than the NETD of the camera (0.02°C) due to the spatial averaging operations. The resulting thermal measurement resolution is a few mK. However, a drift (less than 0.1°C) is observed for the three curves. This is due to thermal disturbances in the specimen's environment;
- $T_{\text{gauge}}(\text{init}) + \theta$ is the “corrected” temperature of the gauge zone after compensation for the drift, where $T_{\text{gauge}}(\text{init})$ is the initial temperature and θ the temperature change calculated as follows [57]:

$$\theta = T_{\text{gauge}} - \frac{T_{\text{ref up}} + T_{\text{ref low}}}{2} - \left(T_{\text{gauge}}(\text{init}) - \frac{T_{\text{ref up}}(\text{init}) + T_{\text{ref low}}(\text{init})}{2} \right) \quad (11)$$

The red curve in Fig. 3-b shows the variations of θ against time. The black dots correspond to the $\langle\theta\rangle$ values averaged every second (leading to a recording frequency f_R of 1 Hz), as will be the case for the processing of the fatigue tests in the next sections. Figure 3-c then gives the variation in the mean heat source $\langle s \rangle$ calculated from Eq. (9). It can be seen that $\langle s \rangle$ fluctuates between about -4000 W/m^3 and 2000 W/m^3 . These values are much lower than those of the mechanical dissipation during fatigue tests, as will be shown in the next sections. Finally, Figure 3-d gives the statistic distribution of $\langle s \rangle$. The standard deviation is equal to about 1200 W/m^3 , which can be considered as a resolution of the heat source measurement.

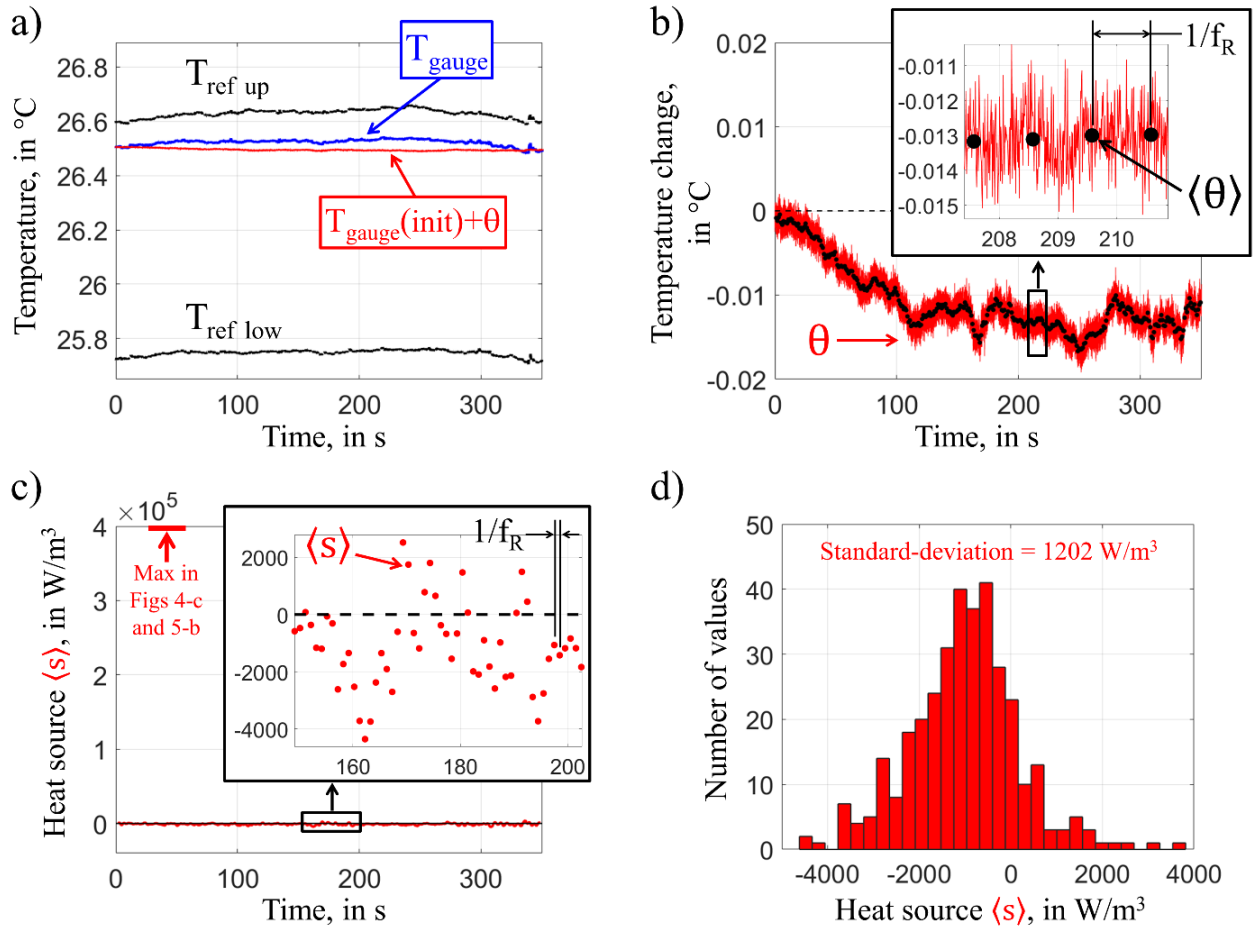


Fig. 3 Identification of the resolution of the heat source measurement from a test without mechanical loading (using the same acquisition conditions as in the fatigue tests).

4. Preliminary simulation

Before presenting the results of the experimental fatigue tests, simulation results are discussed here. The first step consists in creating synthetic temperature changes reproducing the fatigue test presented in Fig. 1. The second step consists in processing these thermal data using HSR.

4.1. Creation of synthetic thermal data

For the simulation, mechanical dissipation d_1 was assumed constant in each cycle. A mathematical model describing the relationship between d_1 and the stress amplitude σ_a was identified for maraging type A steel in Ref [56]: see Eqs (12-14). The relationship is composed

of two regimes. The first regime is described by a quadratic function f_1 , while an exponential trend f_2 is added in the second one, above the material's fatigue limit σ_D :

$$d_1(\sigma_a) = f_1(\sigma_a) + f_2(\sigma_a) \quad (12)$$

with

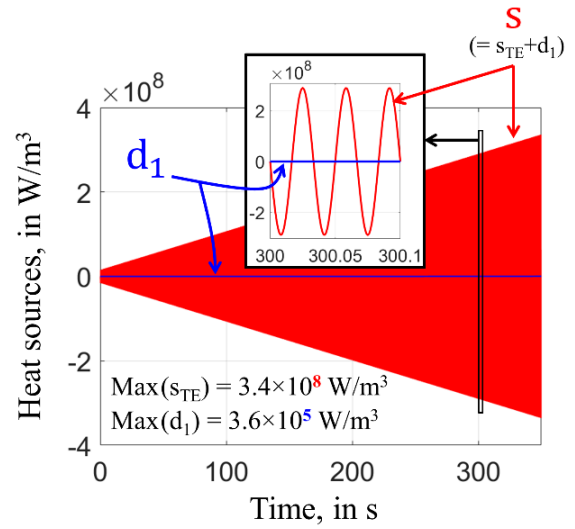
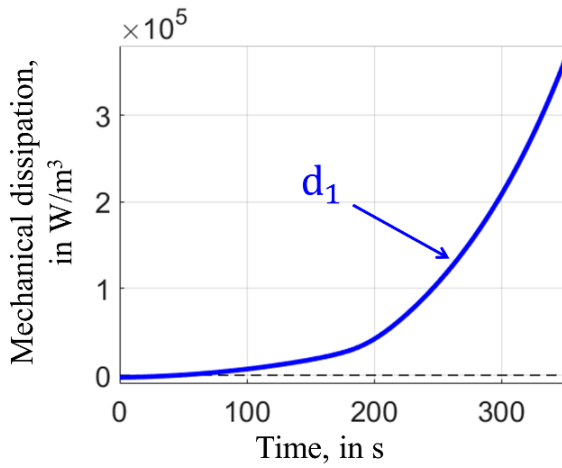
$$f_1(\sigma_a) = a \times \sigma_a^2 \quad (13)$$

$$f_2(\sigma_a) = \begin{cases} 0, & \text{if } \sigma_a < \sigma_D \\ b \times (e^{c \times \sigma_a} - e^{c \times \sigma_D}), & \text{if } \sigma_a \geq \sigma_D \end{cases} \quad (14)$$

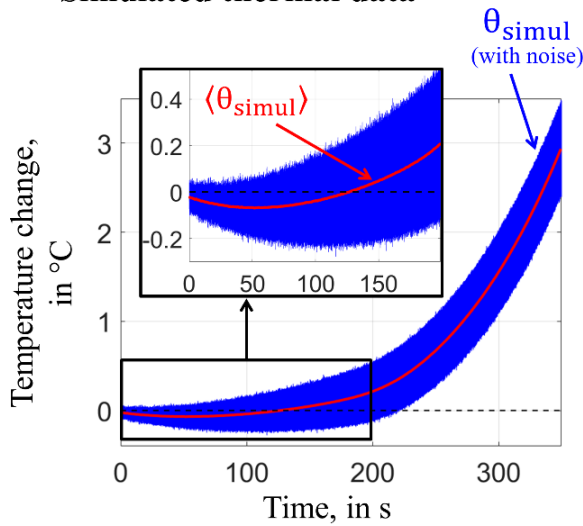
Following parameters were identified for type-A maraging steel: $a = 0.4415 \text{ W.m}^{-3}.\text{MPa}^{-2}$, $b = 1.035.10^4 \text{ W/m}^3$, $c = 0.007081 \text{ MPa}^{-1}$ and $\sigma_D = 281.2 \text{ MPa}$.

Figure 4-a shows the input calorific data of the simulation reproducing the experimental fatigue test. The left graph corresponds to the variation of d_1 against time. The right graph corresponds to the variation of the “total” heat source s (in red), which is composed of the mechanical dissipation term d_1 (in blue) and the thermo-elastic coupling contribution s_{TE} defined by Eq. (1). In agreement with the latter, s_{TE} oscillates at the loading frequency $f_L = 30 \text{ Hz}$, in opposite phase due the minus sign in the formula. It is worth noting that the magnitude of s_{TE} is about three orders higher than that of d_1 . Thermo-elastic coupling is a “strong” coupling. Figure 4-b shows the variation in the temperature change θ_{simul} (in blue) calculated from Eq. (3). For this, a centered finite difference scheme with a time step of 10^{-3} ms was implemented and the calculated data were averaged every 10 ms to create thermal data θ_{simul} at a frequency f_A of 100 Hz. Finally, Gaussian noise with standard deviation of 0.02°C was added to mimic experimental data.

a) **Input calorific data**



b) **Simulated thermal data**



c) **Reconstructed calorific data (at frequency f_R)**

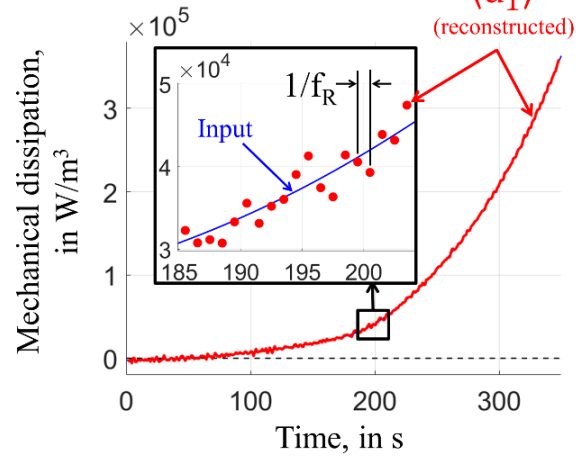


Fig. 4 Simulation of a fatigue test with continuously increasing force amplitude: a) variation in the heat source s composed of a low mechanical dissipation d_1 and a thermo-elastic coupling contribution s_{TE} , b) resulting thermal response, c) reconstructed mechanical dissipation.

4.2. Reconstruction of mechanical dissipation

HSR was then applied to the synthetic noisy thermal data θ_{simul} to retrieve the mechanical dissipation:

- First, θ_{simul} was averaged every $n = 30$ cycles, i.e. every second, leading to a frequency f_R of 1 Hz, as will be the case for the experimental data in the next sections: see the red

curve $\langle \theta_{\text{simul}} \rangle$ in Fig. 4-c. It can be noted that the obtained values are initially slightly negative. This is due to the thermo-elastic coupling contribution before mechanical dissipation becomes preponderant. Indeed, the first mechanical cycle (at $F_{\text{max}} = 500$ N) starts with a stress *increase*: $d\sigma_h/dt(t = 0) > 0$, so $s_{\text{TE}}(t = 0) < 0$. This is why the first value of $\langle \theta_{\text{simul}} \rangle$ is negative: $\langle \theta_{\text{simul}} \rangle_{\text{init}} \approx -0.02^\circ\text{C}$ Furthermore, $\langle s_{\text{TE}} \rangle$ remains negative throughout the test due to the continuously increasing mean stress.

- Second, mean mechanical dissipation $\langle d_1 \rangle$ was calculated using Eqs (7), (9) and (10): see red dots in Fig. 4-c. It appears that the reconstructed mechanical dissipation is very close to the input quantity.

The conclusion might be considered obvious, but it seemed important to illustrate the good reconstruction of the mechanical dissipation despite the high magnitude of the thermo-elastic coupling contribution (about three orders of magnitude as indicated above). Simulations were also used to define the number n of cycles to be used in the averaging operation. A compromise (depending on the ratio F_A/F_L) must actually be found between stress resolution and mechanical dissipation resolution when building the red plot in Fig. 4-c, see also Section 6.

5. Experimental results

This section presents the results of the fatigue tests on maraging and L40 steels (see Table 1). Firstly, Section 5.1 focuses on the results for one maraging specimen for illustration purposes. Secondly, Section 5.2 is dedicated to the comparison between the classical and new procedures for all the specimens tested.

5.1. Focus on one maraging specimen

Before comparing the experimental results between the different specimens in Table 1, Figure 5 focuses on one type-A maraging specimen. Figure 5-a shows the real-time averaged temperature change $\langle \theta \rangle$ at a frequency of 1 Hz. The increase in stress amplitude σ_a per second is 1.35 MPa. During the first 100 seconds, it can be seen that $\langle \theta \rangle$ remains negative; see inset. This is due to the thermo-elastic coupling effect, as also observed in the numerical simulation

in Fig. 4-b. Also, as expected, the first value of $\langle\theta\rangle$ is negative due to the first cycle at $F_{\max} = 500$ N: $\langle\theta\rangle_{\text{init}} = -0.019^\circ\text{C}$. Assuming that there is negligible mechanical dissipation at the beginning of the test, the value of $\langle s_{\text{TE}}\rangle$ can be assessed by the first value of $\langle s\rangle$:

$$\langle s_{\text{TE}}\rangle = \rho C \left[\left(\frac{d\langle\theta\rangle}{dt} \right)_{\text{init}} + \frac{\langle\theta\rangle_{\text{init}}}{\tau} \right] = \rho C \left[-0.001 + \frac{-0.019}{\tau} \right] = -5068 \text{ W/m}^3$$

This value is low compared to the maximum value of $\langle d_1\rangle$ that will be calculated below. It is also in agreement with the theoretical value calculated from Eq. (1) and the value of $d\langle\sigma\rangle/dt$ (which is here a constant, equal to 1.35 MPa/s). It gives the following numerical application, showing a difference of 5.7% compared to the previous approach that may be due to uncertainties in the values of the thermophysical properties of the material:

$$\langle s_{\text{TE}}\rangle = -3 \alpha T_0 \frac{d\langle\sigma_h\rangle}{dt} = -\alpha T_0 \frac{d\langle\sigma\rangle}{dt} = -11.8 \cdot 10^{-6} \times 300 \times 1.35 \cdot 10^6 = -4779 \text{ W/m}^3$$

Figure 5-b shows the variation in mechanical dissipation $\langle d_1\rangle$ as a function of the stress amplitude σ_a , calculated from Eqs (7) and (9). The mechanical dissipation model in Eqs (12-14), which was fitted with the experimental data, is superimposed: see the blue curve. The transition between the two thermal regimes is more clearly visible when plotting the data in log-log scale: see Fig. 5-c. The linear trend of the experimental data in the second regime confirms the exponential trend in natural scale. The noise in the experimental data in log-log scale is due to the fact that the values are small at low stress amplitudes.

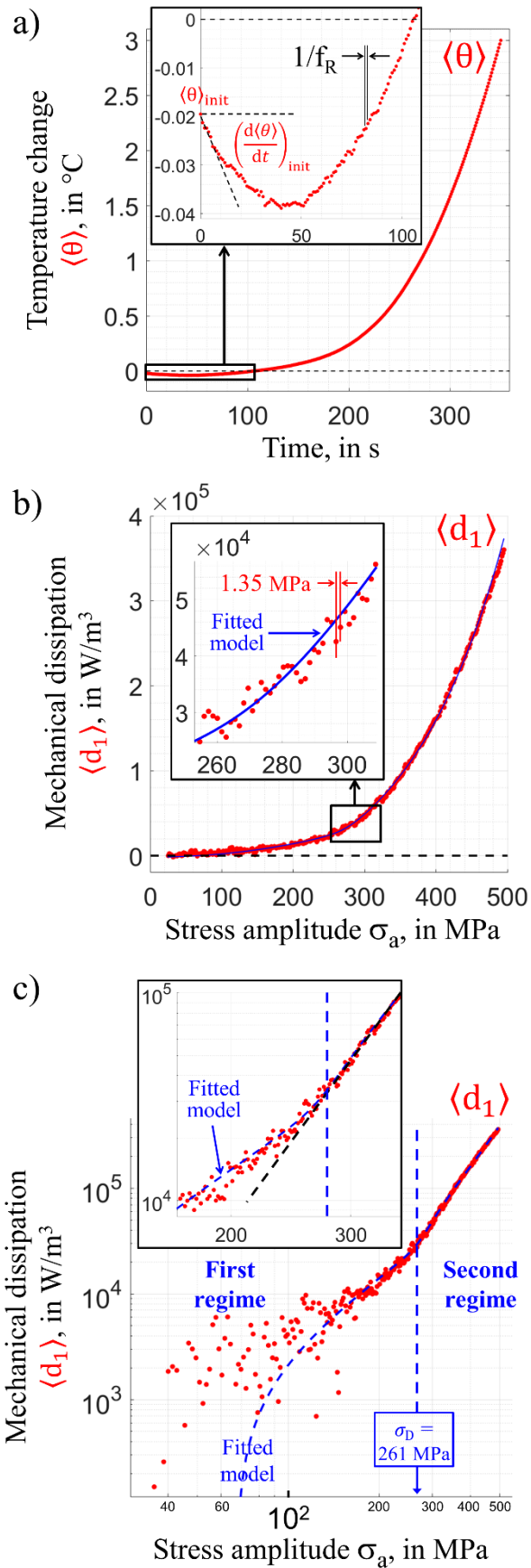


Fig. 5 Experimental results for a type-A maraging specimen: a) thermal response, b) reconstructed mechanical dissipation, c) same in log-log scale.

5.2. Comparison between classical and new loading procedures

This section is dedicated to the core of the study: the comparison between the classical procedure (series of cyclic loading cycles at *constant* amplitudes) and the proposed new procedure (cyclic loading cycles at *continuously varying* amplitudes). In our previous study in Ref [56], we measured the increase in mechanical dissipation using the classical loading procedure for type-A and type-B maraging specimens. The question is whether the new procedure leads to the same results. Figure 6 shows the results of both approaches. Concerning type-A specimens, both approaches give very similar results: the blue curves corresponding to the three samples tested with the new procedure are in the bundle of results obtained with the classical procedure. In addition to the better resolution in stress (one mechanical dissipation value every 1.35 MPa) and the much shorter test duration (less than 6 minutes), it can be noted that the new procedure leads to a maximum stress amplitude which is higher than that of the classical procedure. This is due to a slower accumulation of fatigue damage since it is not necessary to wait for a temperature plateau at each stress amplitude (for the classical procedure, each loading block at constant stress amplitude was applied for 5 minutes). A comment can be made here regarding the type of material tested. If the material exhibits significant cyclic softening or hardening, the mechanical dissipation is not measured in a steady state of cyclic deformation. For example, normalized carbon steels may, at stress amplitudes slightly above the fatigue limit, exhibit elastic cyclic deformation followed by a rapid increase in cyclic plasticity after a few hundred or thousand cycles. Conversely, metastable austenitic Cr-Ni steels may exhibit an endurance limit at about $2 \cdot 10^6$ cycles due to strain-induced martensite formation associated with cyclic hardening [60, 61]. Such effects cannot be fully discerned by the proposed method, which may lead to considerable deviations from more conventional approaches. Concerning the type-B specimens, it can be seen that the results do not coincide as well between the classical and new procedures. However, the difference with the type-A specimen is fairly well rendered by the new procedure, which enables us to rapidly compare printing strategies in terms of fatigue performance. Finally, a comment can be made concerning the fatigue limit values identified using the new procedure: see Table 3. Identification was performed by fitting the calorific data with the model in Eqs (12-14) to find the value of the fatigue limit σ_D of the material. For type-A maraging, the values in Table 3 are the average over the different specimens tested (14 for the classical procedure, 3 for the new procedure). The

mean value for type-A maraging appears to be very close to that found with the classical approach. The excellent agreement between the two procedures could be a coincidence, given the small number of specimens and the large dispersion of the data. A large discrepancy is observed for type-B maraging, which could be explained by the small number of specimens tested (3 for the classical procedure, 1 for the new procedure) and a high porosity level leading to a more critical variability of the results.

Table 3 Comparison of the average fatigue limit values for maraging steels between the classical and new procedures. Number of specimens for type A: 14 for the classical procedure, 3 for the new procedure. Number of specimens for type B: 3 for the classic procedure, 1 for the new procedure..

	Fatigue limit identified by	
	classical procedure [56]	new procedure
Type-A maraging	255 MPa	254 MPa
Type-B maraging	106 MPa	140 MPa

A comparison was also made for the L40 specimens: see Fig. 7. It can be noted first that the order of magnitude of mechanical dissipation is about one order lower than that of the maraging steels (maximum equal to about $6 \cdot 10^4 \text{ W/m}^3$ and $6 \cdot 10^5 \text{ W/m}^3$ respectively). The signal-to-noise ratio is therefore *a priori* penalizing for the accuracy of the mechanical dissipation measurement. However, it can be seen from the graph that the classical and new approaches give very close results. Based on the results for the two types of materials, the new loading procedure coupled with HSR is found to be effective in measuring the relationship between mechanical dissipation and stress magnitude. The next section provides additional information about the data processing.

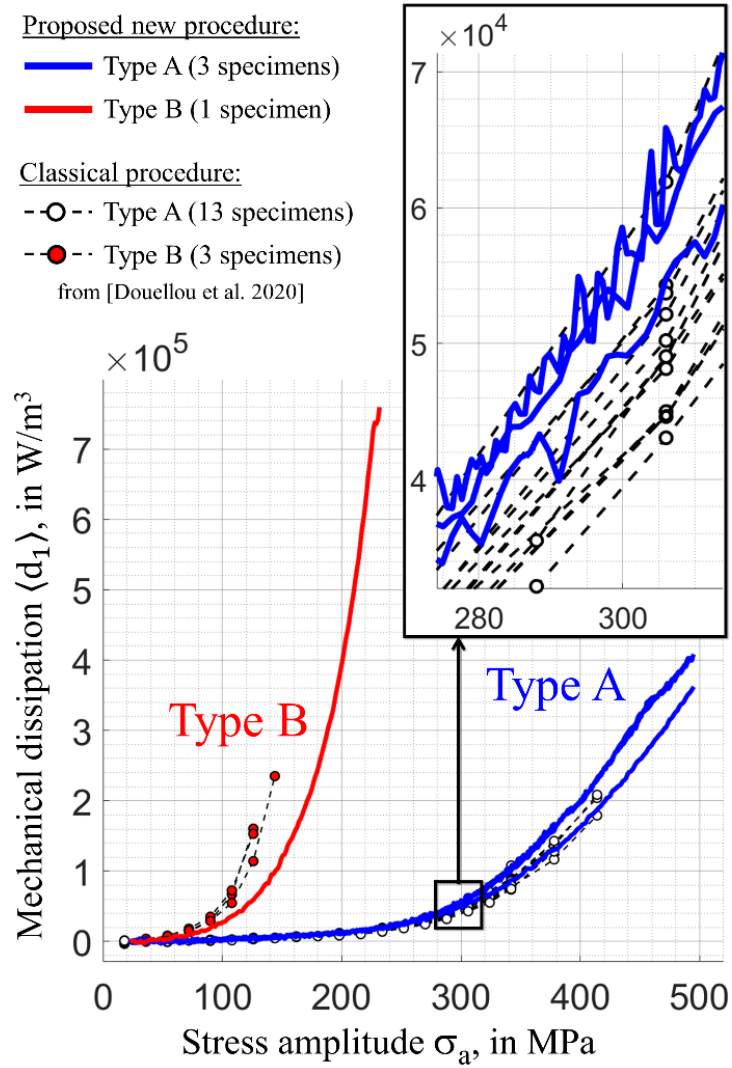


Fig. 6 Comparison between the classical procedure and the proposed new approach for the two types of maraging steels (see Table 1).

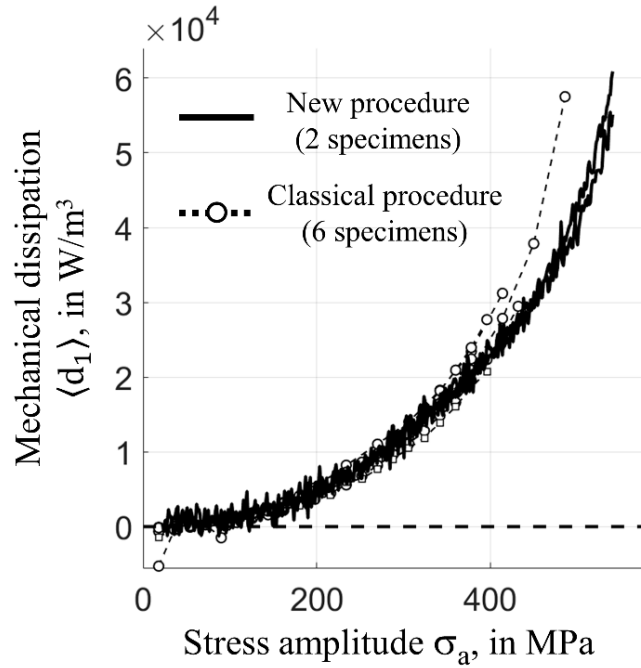


Fig. 7 Results for L40 steels featuring very low mechanical dissipation (about 10 times lower than for maraging steels).

6. Additional comments

Before concluding this study, additional comments are now provided about the data processing, and in particular about the relevance of the real-time averaging operation. Calculating the mean mechanical dissipation $\langle d_1 \rangle$ using θ from Eqs (7) and (8) or using $\langle \theta \rangle$ from Eqs (7) and (9) is theoretically equivalent. However, the latter solution is in practice more precise (in addition to generating much smaller acquisition files). A comparison was made to illustrate this point. A test on a type-A maraging steel was performed at an acquisition frequency f_A of 120 Hz *without* real-time average recording. An averaging operation to obtain $\langle \theta \rangle$ at the frequency f_R of 1 Hz (i.e. every 30 cycles) was performed in post-processing. Figure 8-a shows the variation in temperature change θ at 120 Hz (in blue). The red curve corresponds to the mean temperature change $\langle \theta \rangle$ at 1 Hz. By construction, the blue curve cannot correctly “capture” the amplitude of the temperature fluctuation associated with the thermo-elastic coupling effect. Indeed, there are here only 4 temperature values per cycle ($f_A/f_L = 4$). However, by construction, the variation in the mean temperature change $\langle \theta \rangle$ is correctly captured. Note that when F_A is not a multiple of F_L (as in the previous sections), the variation in $\langle \theta \rangle$ can be also correctly captured using

several cycles. Figure 8-b gives the mean mechanical dissipation $\langle d_1 \rangle$ obtained from two processing procedures:

- P1: from the heat sources calculated at 120 Hz and averaged afterwards (in blue);
- P2: from the averaged thermal data at 1 Hz (in red).

It can be seen that processing P1 leads to large errors in certain zones of the graph: see in particular between 360 MPa et 400 MPa. These errors are due to missing images during acquisition. In this case, the calculated thermo-elastic sources do not vanish over a mechanical cycle, which leads to significant errors. Apart from these large errors, it appears that processing P1 leads to slightly more noise than processing P2. This noise can be better evidenced in log-log scale: see Fig. 8-c. The slightly higher noise can be explained by the resolution of the time base that plays an important role in the calculation of the time derivative $d\theta/dt$ by finite differences in the heat equation.

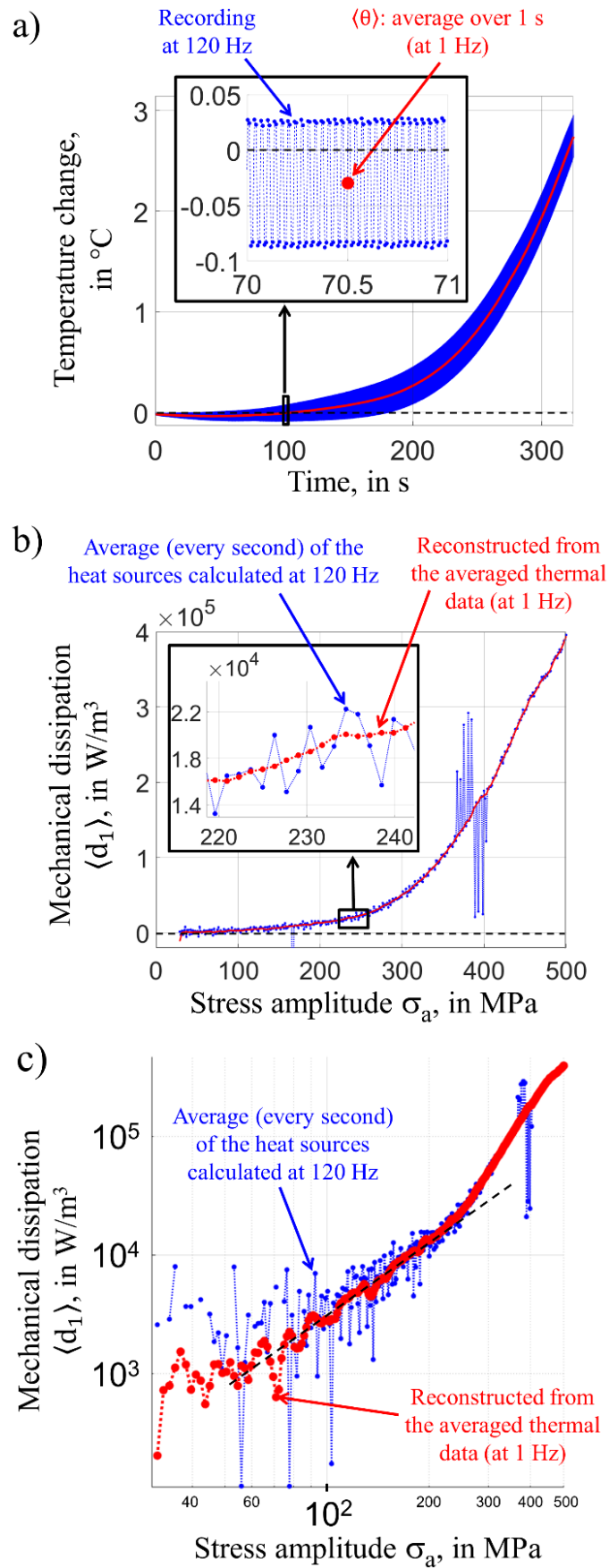


Fig. 8 Processing from thermal data recorded at 120 Hz (illustration for a type-A maraging specimen).

7. Conclusion

Over the past decades, self-heating measurements by IR thermography have proven to be an effective way to rapidly evaluate the fatigue response of various types of materials. In addition, calculating mechanical dissipation from the measured temperatures is a relevant way of analyzing a quantity that is directly associated with fatigue damage. In this study, we have proposed to apply HSR in the case of cyclic loading with *continuously varying* stress amplitude in order to obtain a “continuous” relationship between mechanical dissipation and stress amplitude. We compared the results with those of the classical approach (a series of cyclic loading blocks with *constant* stress amplitudes) for two types of AM steels, which allowed us to validate the new proposed procedure. The following advantages of the new procedure can be highlighted:

- the test time is considerably reduced compared to the classical procedure. In the present study, the duration of the fatigue characterization was about 6 minutes;
- the stress resolution (in the relationship between stress amplitude and mechanical dissipation) is improved. In the present study, one mechanical dissipation value was measured every 1.35 MPa. A better stress resolution provides more data for a better identification of the transition between the two mechanical dissipation regimes (*i.e.* below and above the fatigue limit);
- A higher maximum stress amplitude can be reached. This is due to a slower accumulation of fatigue damage during the test since it is not necessary to wait for a temperature plateau at each stress amplitude value. Achieving a higher stress level enables increased data acquisition in the second regime (above the fatigue limit), which may facilitate the identification of the fatigue limit in some cases.

The perspective for the study is to apply the procedure to a wide range of materials, in particular AM materials. The latter are particularly targeted in order to perform an optimization of manufacturing parameters with respect to fatigue performance. This can now be envisaged thanks to the short duration of the characterization procedure proposed in this study.

Declaration of Competing Interest

The authors declare that they have no known competing financial interests or personal relationships that could have appeared to influence the work reported in this paper.

Acknowledgments

The authors acknowledge the Région Auvergne-Rhône-Alpes for the support in this study (Project: IRICE Fabrication additive, number: 18 009727 01-59941, operation: P088O005). The authors would like to thank Mr. Alexis Gravier, Sigma Clermont engineering school, for setting up the experimental mechanical procedure.

References

- [1] Blinn B, Beck T, Jost B, Klein M, Eifler D. PhyBaL(SL) - Short-time procedure for the determination of the fatigue lifetime of metallic materials under service loading. *Int J Fatigue* 2021;144:106060. <https://doi.org/10.1016/j.ijfatigue.2020.106060>
- [2] Starke P, Walther F, Eifler D. Fatigue assessment and fatigue life calculation of quenched and tempered SAE 4140 steel based on stress-strain hysteresis, temperature and electrical resistance measurements. *Fatigue Fract Eng Mater Struct* 2007;30:1044–51. <https://doi.org/10.1111/j.1460-2695.2007.01174.x>
- [3] Stromeyer CE. The determination of fatigue limits under alternating stress conditions. *Proc R Soc Lond A* 1914;90:411–25. <https://doi.org/10.1098/rspa.1914.0066>
- [4] Luong MP. Infrared thermographic scanning of fatigue in metals. *Nucl Eng Des* 1995;158:363–76. [https://doi.org/10.1016/0029-5493\(95\)01043-H](https://doi.org/10.1016/0029-5493(95)01043-H)
- [5] Luong MP. Fatigue limit evaluation of metals using an infrared thermographic technique. *Mech Mater* 1998;28:155–63. [https://doi.org/10.1016/S0167-6636\(97\)00047-1](https://doi.org/10.1016/S0167-6636(97)00047-1)
- [6] La Rosa G, Risitano A. Thermographic methodology for rapid determination of the fatigue limit of materials and mechanical components. *Int J Fatigue* 2000;22:65–73. [https://doi.org/10.1016/S0142-1123\(99\)00088-2](https://doi.org/10.1016/S0142-1123(99)00088-2)
- [7] Geraci AL, La Rosa G, Risitano A, Grech M. Determination of the fatigue limit of an austempered ductile iron using thermal infrared imagery. In: Fedosov E.A. (ed.) *Proceedings of SPIE. Digital Photogrammetry and Remote Sensing '95, Moscow, Russia, June 25-30, 1995, Vol. 2646, pp. 306–317, 1995.* <https://doi.org/10.1117/12.227882>

- [8] Huang J, Pastor ML, Garnier C, Gong X. Rapid evaluation of fatigue limit on thermographic data analysis. *Int J Fatigue* 2017;104:293–301. <https://doi.org/10.1016/j.ijfatigue.2017.07.029>
- [9] De Finis R, Palumbo D, da Silva MM, Galietti U. Is the temperature plateau of a self-heating test a robust parameter to investigate the fatigue limit of steels with thermography? *Fatigue Fract Eng Mater Struct* 2018;41:917–34. <https://doi.org/10.1111/ffe.12738>
- [10] Munier R, Doudard C, Calloch S, Weber B. Identification of the micro-plasticity mechanisms at the origin of self-heating under cyclic loading with low stress amplitude. *Int J Fatigue* 2017;103:122–35. <https://doi.org/10.1016/j.ijfatigue.2017.05.027>
- [11] Munier R, Doudard C, Calloch S, Weber B. Determination of high cycle fatigue properties of a wide range of steel sheet grades from self-heating measurements. *Int J Fatigue* 2014;63:46–61, 2014. <https://doi.org/10.1016/j.ijfatigue.2014.01.004>
- [12] De Finis R, Palumbo D, Ancona F, Galietti U. Fatigue limit evaluation of various martensitic stainless steels with new robust thermographic data analysis. *Int J Fatigue* 2015;74:88–96. <https://doi.org/10.1016/j.ijfatigue.2014.12.010>
- [13] Cao YF, Moumni Z, Zhu JH, Zhang YH, You YJ, Zhang WH. Comparative investigation of the fatigue limit of additive-manufactured and rolled 316 steel based on self-heating approach. *Eng Fracture Mech* 2020;223:106746. <https://doi.org/10.1016/j.engfracmech.2019.106746>
- [14] Shiozawa D, Inagawa T, Washio T, Sakagami T. Fatigue limit estimation of stainless steels with new dissipated energy data analysis. *Procedia Struct Integrity* 2016;2:2091–96. <https://doi.org/10.1016/j.prostr.2016.06.262>
- [15] De Finis R, Palumbo D, Galietti U. A multianalysis thermography-based approach for fatigue and damage investigations of ASTM A182 F6NM steel at two stress ratios. *Fatigue Fract Eng Mater Struct* 2019;42(1):267–283. <https://doi.org/10.1111/ffe.12903>
- [16] Meneghetti G. Analysis of the fatigue strength of a stainless steel based on the energy dissipation. *Int J Fatigue* 2007;29(1):81–94. <https://doi.org/10.1016/j.ijfatigue.2006.02.043>
- [17] Pessard E, Morel F, Verdu C, Flaceliere L, Baudry G. Microstructural heterogeneities and fatigue anisotropy of forged steels. *Mater Sci Eng A* 2011;529:289–99. <https://doi.org/10.1016/j.msea.2011.09.031>

- [18] Rigon D, Berto F, Meneghetti G. Estimating the multiaxial fatigue behaviour of C45 steel specimens by using the energy dissipation. *Int J Fatigue* 2021;151:106381. <https://doi.org/10.1016/j.ijfatigue.2021.106381>
- [19] Bercelli L, Moynes S, Dhondt M, Doudard C, Calloch S, Beaudet J. A probabilistic approach for high cycle fatigue of Wire and Arc Additive Manufactured parts taking into account process-induced pores. *Addit Manuf* 2021;42:101989. <https://doi.org/10.1016/j.addma.2021.101989>
- [20] Yang WP, Guo XL, Guo Q, Fan JL. Rapid evaluation for high-cycle fatigue reliability of metallic materials through quantitative thermography methodology. *Int J Fatigue* 2019;124:461–72. <https://doi.org/10.1016/j.ijfatigue.2019.03.024>
- [21] Facchinetti M, Florin P, Doudard C, Calloch S. Identification of Self-Heating Phenomena Under Cyclic Loadings Using Full-Field Thermal and Kinematic Measurements: Application to High-Cycle Fatigue of Seam Weld Joints. *Exp Mech* 2015;55:681–98. <https://doi.org/10.1007/s11340-013-9835-1>
- [22] Guo Q, Zairi F, Yang WP. Evaluation of intrinsic dissipation based on self-heating effect in high-cycle metal fatigue. *Int J Fatigue* 2020;139:105653. <https://doi.org/10.1016/j.ijfatigue.2020.105653>
- [23] Maquin F, Pierron F. Heat dissipation measurements in low stress cyclic loading of metallic materials: From internal friction to micro-plasticity. *Mech Mater* 2009;41:928–42. <https://doi.org/10.1016/j.mechmat.2009.03.003>
- [24] De Finis R, Palumbo D, Serio LM, De Filippis LAC, Galietti U. Correlation between Thermal Behaviour of AA5754-H111 during Fatigue Loading and Fatigue Strength at Fixed Number of Cycles. *Materials* 2018;11:719. <https://doi.org/10.3390/ma11050719>
- [25] Guo SF, Liu XS, Zhang HX, Yan ZF, Zhang ZD, Fang HY. Thermographic study of AZ31B magnesium alloy under cyclic loading: temperature evolution analysis and fatigue limit estimation. *Materials* 2020;13:5209. <https://doi.org/10.3390/ma13225209>
- [26] Guo SF, Liu XS, Zhang HX, Yan ZF, Fang HY. Fatigue limit evaluation of AZ31B magnesium alloy based on temperature distribution analysis. *Metals* 2020;10:1331. <https://doi.org/10.3390/met10101331>
- [27] Guo SF, Liu XS, Zhang HX, Yan ZF, Fang HY. Fatigue Performance Evaluation of AZ31B Magnesium Alloy Based on Statistical Analysis of Self-Heating. *Materials* 2021;14:2251. <https://doi.org/10.3390/ma14092251>

- [28] Jongchansitto P, Douellou C, Preechawuttipong I, Balandraud X. Comparison between 0D and 1D approaches for mechanical dissipation measurement during fatigue tests. *Strain* 2019;55:e12307. <https://doi.org/10.1111/str.12307>
- [29] Wang XG, Crupi V, Jiang C, Feng ES, Guglielmino E, Wang CS. Energy-based approach for fatigue life prediction of pure copper. *Int J Fatigue* 2017;104:243–50. <https://doi.org/10.1016/j.ijfatigue.2017.07.025>
- [30] Ezanno A, Doudard C, Calloch S, Heuze JL. A new approach to characterizing and modeling the high cycle fatigue properties of cast materials based on self-heating measurements under cyclic loadings. *Int J Fatigue* 2013;47:232–43. <https://doi.org/10.1016/j.ijfatigue.2012.09.005>
- [31] Akai A, Shiozawa D, Sakagami T. Fatigue limit estimation of titanium alloy Ti-6Al-4V with infrared thermography. In: Bison P, Burleigh D (eds) *Thermosense: Thermal Infrared Applications XXXIX*. Proceedings of SPIE, Vol. 10214, UNSP 102141J, SPIE-Int Soc Optical Engineering, Bellingham, WA, USA, 2017. <https://doi.org/10.1117/12.2263843>
- [32] Mostofizadeh P, Kadkhodaei M, Chirani SA, Saint-Sulpice L, Rokbani M, Bouraoui T, Calloch S. Fatigue analysis of shape memory alloys by self-heating method. *Int J Mech Sci* 2019;156:329–41. <https://doi.org/10.1016/j.ijmecsci.2019.04.012>
- [33] Bayati P, Jahadakbar A, Barati M, Nematollahi M, Saint-Sulpice L, Haghshenas M, Chirani SA, Mahtabi MJ, Elahinia M. Toward low and high cycle fatigue behavior of SLM-fabricated NiTi: Considering the effect of build orientation and employing a self-heating approach. *Int J Mech Sci* 2020;185:105878. <https://doi.org/10.1016/j.ijmecsci.2020.105878>
- [34] Rokbani M, Saint-Sulpice L, Chirani SA, Bouraoui T. Fatigue properties by “self-heating” method: Application to orthodontic Ni-Ti wires after hydrogen charging. *J Intell Mater Syst Struct* 2018;29:3242–53. <https://doi.org/10.1177/1045389X18778371>
- [35] Rokbani M, Saint-Sulpice L, Chirani SA, Bouraoui T. Hydrogen effects on Ni-Ti fatigue performance by self-heating method. *Smart Mater Struct* 2017;26:105016. <https://doi.org/10.1088/1361-665X/aa86f4>
- [36] Barati M, Amini B, Segouin V, Daniel L, Chirani SA, Calloch S. Investigation of self-heating and dissipative effects in ferroelectric ceramics subjected to compressive mechanical cyclic loading. *Acta Mater* 2021;221:117386. <https://doi.org/10.1016/j.actamat.2021.117386>

- [37] De Finis R, Palumbo D, Galietti U. Fatigue damage analysis of composite materials using thermography-based techniques. *Procedia Struct Integrity* 2019;18:781–91. <https://doi.org/10.1016/j.prostr.2019.08.227>
- [38] Palumbo D, De Finis R, Demelio PG, Galietti U. A new rapid thermographic method to assess the fatigue limit in GFRP composites. *Composites, Part B* 2016;103:60–7. <https://doi.org/10.1016/j.compositesb.2016.08.007>
- [39] De Finis R, Palumbo D. Estimation of the dissipative heat sources related to the total energy input of a CFRP composite by using the second amplitude harmonic of the thermal signal. *Materials* 2020;13:28250. <https://doi.org/10.3390/ma13122820>
- [40] Mirzaei AH, Shokrieh MM. Simulation and measurement of the self-heating phenomenon of carbon/ epoxy laminated composites under fatigue loading. *Composites Part B* 2021;223:109097. <https://doi.org/10.1016/j.compositesb.2021.109097>
- [41] Chrysochoos A, Chezeaux JC, Caumon H. Thermomechanical behavior law analysis by infrared thermography. *Revue de Physique Appliquée* 1989;24:215–25. <https://doi.org/10.1051/rphysap:01989002402021500>
- [42] Chrysochoos A, Maisonneuve O, Martin G, Caumon H, Chezeaux JC. Plastic and dissipated work and stored energy. *Nucl Eng Des* 1989;114:323–33. [https://doi.org/10.1016/0029-5493\(89\)90110-6](https://doi.org/10.1016/0029-5493(89)90110-6)
- [43] Chrysochoos A, Peyroux R. Experimental analysis and numerical simulation of thermomechanical couplings in solid materials. *Revue Générale de Thermique* 1998;37:582–606. [https://doi.org/10.1016/S0035-3159\(98\)80036-6](https://doi.org/10.1016/S0035-3159(98)80036-6)
- [44] Chrysochoos A, Louche H. An infrared image processing to analyse the calorific effects accompanying strain localisation. *Int J Eng Sci* 2000;38:1759–88. [https://doi.org/10.1016/S0020-7225\(00\)00002-1](https://doi.org/10.1016/S0020-7225(00)00002-1)
- [45] Boulanger T, Chrysochoos A, Mabru C, Galtier C. Calorimetric analysis of dissipative and thermoelastic effects associated with the fatigue behavior of steels. *Int J Fatigue*. 2006;26:221–29. [https://doi.org/10.1016/S0142-1123\(03\)00171-3](https://doi.org/10.1016/S0142-1123(03)00171-3)
- [46] Chrysochoos A, Berthel B, Latourte F, Galtier A, Pagano S, Wattrisse B. Local energy analysis of high-cycle fatigue using digital image correlation and infrared thermography. *J Strain Anal Eng Des* 2008;43:411–21. <https://doi.org/10.1243/03093247JSA374>
- [47] Chrysochoos A, Berthel B, Latourte F, Pagano S, Wattrisse B, Weber B. Local energy approach to steel fatigue. *Strain* 2008;44:327–34. <https://doi.org/10.1111/j.1475-1305.2007.00381.x>

- [48] Berthel B, Wattrisse B, Chrysochoos A, Galtier A. Thermographic analysis of fatigue dissipation properties of steel sheets. *Strain* 2007;43:273–79.
<https://doi.org/10.1111/j.1475-1305.2007.00349.x>
- [49] Morabito AE, Chrysochoos A, Dattoma V, Galietti U. Analysis of heat sources accompanying the fatigue of 2024 T3 aluminium alloys. *Int J Fatigue*. 2007;29(5):977–84. <https://doi.org/10.1016/j.ijfatigue.2006.06.015>
- [50] Giancane S, Chrysochoos A, Dattoma V, Wattrisse B. Deformation and dissipated energies for high cycle fatigue of 2024-T3 aluminium alloy. *Theor Appl Fract Mech* 2009;52:117–21. <https://doi.org/10.1016/j.tafmec.2009.08.004>
- [51] Favier V, Blanche A, Wang C, Phung NL, Ranc N, Wagner D, Bathias C, Chrysochoos A, Mughrabi H. Very high cycle fatigue for single phase ductile materials: Comparison between alpha-iron, copper and alpha-brass polycrystals. *Int J Fatigue* 2016;93:326–38. <https://doi.org/10.1016/j.ijfatigue.2016.05.034>
- [52] Blanche A, Chrysochoos A, Ranc N, Favier V. Dissipation assessments during dynamic very high cycle fatigue tests. *Exp Mech* 2015;55:699–709.
<https://doi.org/10.1007/s11340-014-9857-3>
- [53] Benaarbia A, Chrysochoos A, Robert G. Thermomechanical behavior of PA6.6 composites subjected to low cycle fatigue. *Composites Part B* 2015;76:52–64.
<https://doi.org/10.1016/j.compositesb.2015.02.011>
- [54] Benaarbia A, Chrysochoos A, Robert G. Fiber orientation effects on heat source distribution in reinforced polyamide 6.6 subjected to low cycle fatigue. *J Eng Math* 2015;90:13–36. <https://doi.org/10.1007/s10665-014-9720-7>
- [55] Berthel B, Chrysochoos A, Wattrisse B, Galtier A. Infrared image processing for the calorimetric analysis of fatigue phenomena. *Exp Mech* 2008;48:79–90.
<https://doi.org/10.1007/s11340-007-9092-2>
- [56] Douellou C, Balandraud X, Duc E, Verquin B, Lefebvre F, Sar F. Rapid characterization of the fatigue limit of additive-manufactured maraging steels using infrared measurements. *Additive Manufacturing* 2020;35:101310.
<https://doi.org/10.1016/j.addma.2020.101310>
- [57] Delpueyo D, Balandraud X, Grédiac M, Stanciu S, Cimpoesu N. A specific device for enhanced measurement of mechanical dissipation in specimens subjected to long-term tensile tests in fatigue. *Strain* 2018;54:e12252. <https://doi.org/10.1111/str.12252>
- [58] Douellou C. Fatigue des aciers élaborés par fabrication additive L-PBF : approche thermomécanique et comparaison de stratégies de fabrication. In French. PhD thesis

report. Université Clermont Auvergne (2020). <https://tel.archives-ouvertes.fr/tel-03023001/document>

- [59] Dulieu-Barton JM, Stanley P. Development and applications of thermoelastic stress analysis. *J Strain Anal Eng Des* 1998;33:93–104. <https://doi.org/10.1243/0309324981512841>
- [60] Muller-Bollenhagen C, Zimmermann M, Christ HJ. Very high cycle fatigue behaviour of austenitic stainless steel and the effect of strain-induced martensite. *Int J Fatigue* 2021;32:936–42. <https://doi.org/10.1016/j.ijfatigue.2009.05.007>
- [61] Smaga M, Boemke A, Daniel T, Skorupski R, Sorich A, Beck T. Fatigue behavior of metastable austenitic stainless steels in LCF, HCF and VHCF regimes at ambient and elevated temperatures. *Metals* 2019;9:704. <https://doi.org/10.3390/met9060704>